Graphene wrapped MXene *via* plasma exfoliation for all-solid-state flexible supercapacitors

Keliang Wang [a,b,*], Bocong Zheng [a,b], Madeline Mackinder [b], Nina Baule [a], Hui Qiao [c], Hong Jin [d], Thomas Schuelke [b], Qi Hua Fan [b,**]

[a] *Fraunhofer USA, Inc. Center for Coatings and Diamond Technologies, Michigan State University, East Lansing, MI, 48824, USA*
[b] *Department of Electrical Engineering and Computer Engineering & Department of Chemical Engineering and Materials Science, Michigan State University, East Lansing, MI, 48824, United States*
[c] *Key Laboratory of Eco-textiles, Ministry of Education, Jiangnan University, Wuxi, 214122, People's Republic of China*
[d] *Suzhou Research Institute, Xi'an Jiaotong University, Suzhou, 215123, People's Republic of China*

ARTICLE INFO

ABSTRACT

Two dimensional transition metal carbides and nitrides, known as MXenes, are promising materials for energy storage. Although superior capacitance performance has been demonstrated using MXene electrodes in supercapacitors, the relatively high resistance and inefficient separation process limit the materials applications. This work reports an innovative facile method combined with plasma exfoliation to fabricating graphene-wrapped MXene. This method includes two key aspects: 1) incorporating graphite oxide (GO) into MXene, and 2) plasma exfoliating of GO-modified MXene. The resulting materials, denoted as MXene@rGO, have a layered structure with reduced graphene on the MXene surfaces. All-solid-state flexible supercapacitors have been fabricated using the MXene@rGO materials. Comparing to regular MXene, the MXene@rGO supercapacitors exhibited two times higher specific capacitance as well as excellent charge/discharge and mechanical stability. This research has the potential to lead to the development of new electrode materials that significantly promote the capacity of energy storage.

1. Introduction

Flexible electronic devices have attracted great interest in recent years [1–3]. Among these devices, flexible supercapacitors are the potential energy storage components for powering wearable, portable, and foldable electronics [4]. Compared to the other power sources, supercapacitors present unique merits including fast charge/discharge rate, high power density, and long cycling life. The capacitance performance of supercapacitors is critical to the applications and essentially depends on the properties of the electrode materials. The common electrode materials for supercapacitors include carbon-based materials (*e.g.* activated carbon, carbon nanotube, graphene, etc.) for electrical double layer capacitors (EDLCs) [5–7] and metal oxides (*e.g.* RuO_2, MnO_2), nitrides and carbides for pseudocapacitors [8–17]. The increasing demand for high-capacity energy storage has been continuously driving the exploration of novel electrode materials and efficient manufacturing methods.

A class of two-dimensional (2D) metal carbide and nitride materials denoted as MXene have emerged recently and have been demonstrated with great potential for high-capacity energy storage [18]. MXene has been derived from its parent phase MAX, where *M* represents the early transition metals (*e.g.* Ti, Mo), *A* stands for the elements in group IIIA or IVA (*e.g.* Al, Ga), and *X* is C or N. The reported method to obtain MXene includes selectively etching to remove element *A* in the MAX phase and create 2D materials with a general formula of $M_{n+1}X_nT_x$, where *T* is a functional group [19–21]. MXene features layered structures with expanded interlayer spacing, which offers large surface areas and active surface sites. MXene has been demonstrated with comparable energy storage performance as graphene [21–25].

As other 2D materials, as-derived MXene nanosheets tend to agglomerate and restack, which limits the accessible surface areas. Hence, exfoliating multilayered MXene into fewer layers or even single layers is necessary. However, using regular mechanical method (*e.g.* Scotch tape [26,27]) to exfoliate MXene is inefficient because the interlayer interactions are 2–6 fold greater than those in graphite and bulk

---

MoS_2 [28]. A variety of strategies have been reported to prevent the agglomeration and restacking of 2D materials, such as 1) electrostatic self-assembly based on the surface charge (*e. g.* Ref. [25] for graphene, [29] for carbon nanotube); and 2) intercalating polar or large organic molecules to the MXene surfaces [30–32]. The processes include a series of mechanical sonication to create single- and multi-layered MXene colloidal solutions. With subsequent filtration, freestanding MXene can be obtained. The intercalation usually leads to reduced electric conductivity and capacitance performance due to the introduction of the organic or other non-conductive molecules in the MXene surfaces [33,34]. The intercalation involves complicated separation processes. Hence, more effective method is needed to exfoliate MXene.

This paper reports a new plasma excitation method to efficiently exfoliate MXene and simultaneously wrap the exfoliated nanosheets with graphene. Industry plasmas, also called low-temperature plasmas, are usually generated by strong electromagnetic fields. Free electrons driven by the electric field gain kinetic energy and interact with the background gas molecules. The average electron energy is a few eV (1 eV = 11,594 K), depending on the plasma excitation process. The energetic electrons can dissociate, ionize, or excite the gas molecules. As a result, a large number of gas ions, atoms, and excited species are created in the plasma. These gas species are highly reactive and can intensively interact with the sample materials and enable the exfoliation of graphite oxides [35].

This method eliminates the intercalation process [21,36]. The idea is inspired by our previous work [37,38], which shows that graphite oxide (GO) can be efficiently exfoliated by CH_4 plasmas and reduced into graphene oxide (rGO). In the preparation of MXene, GO colloid serves as a binder to cover the surface and reach into the interlayers of MXene. Upon CH_4 plasma excitation, the GO binder expands due to the breakdown of the C—O bonds and the MXene is exfoliated. After the exfoliation, MXene is transformed into rGO-wrapped MXene composite. The resulting 2D materials are subsequently used in all-solid-state flexible supercapacitors, which demonstrate that the addition of rGO significantly boosts the electrochemical performance of MXene.

2. Experimental

2.1. Preparation of MXene

MAX phase of Ti_3AlC_2 was used as the precursor to prepare MXene, $Ti_3C_2T_x$, according to a previous report [18]. Typically, 1 g Ti_3AlC_2 powder was dispersed into 10 ml hydrofluoric acid (HF, 48 *wt*%, Fisher Scientific Inc.) under vigorous stirring at room temperature for 24 h. The suspension was then centrifuged at 4000 rpm for 5 min each time until the pH of the supernatant was close to 7. The sediment was collected and dried in an oven at $60\,°C$ overnight. The prepared sample was denoted as MXene. It should be noted that the handling of HF acid must comply with the rules of environmental health and safety due to its hazardous nature.

2.2. Preparation of graphite oxides

Graphite oxides (GOs) were prepared by oxidizing graphite using a modified Hummers' method reported in previous works [39]. Typically, Graphite flakes (2.5 g, Fisher Scientific Inc.) were mixed with concentrated sulfuric acid (H_2SO_4, 98 *wt*%, 75 ml, Fisher Scientific Inc.) under vigorous stirring at $0\,°C$ for 4 h. Then, sodium nitrate ($NaNO_3$, 1.25 g, Fisher Scientific Inc.) and potassium permanganate ($KMnO_4$, 7.5 g, Fisher Scientific Inc.) were slowly added in sequence. After 12 h of reaction at room temperature, 25 ml deionized water was slowly added into the mixture and the temperature was increased to $98\,°C$ before an additional 75 ml of deionized water was added. After 4 h, 7.5 ml of hydrogen peroxide (H_2O_2, 30 *wt*%, Fisher Scientific Inc.) was dropwise added and a yellow colloid was formed. Then, the mixture was transferred into several dialysis tubes (14,000 MWCO Daltons, Fisher Scientific Inc.) to dialyze in deionized water for 7 days until the pH was close to 7. The

dialyzed sample was then stored in a refrigerator and denoted as GO.

2.3. Preparation of graphene oxide covered MXene sheets

100 mg MXene powder and 5 ml GO colloid solution were added into 50 ml DI water. The mixture was then homogenized by a homogenizer (Pro25D, Pro Scientific Inc.) at a speed of 12000 rpm for 2 min. Then, the dispersion was poured into 3 Petri dishes (100 mm diameter × 15 mm height, Fisher Scientific Inc.) and then horizontally placed into a fume hood to dry naturally. After drying, the formed sheet films could be easily peeled off and denoted as MXene@GO.

2.4. Preparation of graphene wrapped MXene

Graphene wrapped MXene was prepared using a dielectric barrier discharge plasma system powered by a 13.56 MHz RF power supply. The prepared MXene@GO sheet was put into a quartz tube plasma reactor, which was evacuated and purged several times with the processing gas CH_4 to remove the residual air in the tube. Then, the gas flow rate was set to 100 sccm and the pressure was maintained at 2 Torr by adjusting an exit vacuum valve linked to a pump. The RF power was subsequently introduced to generate a plasma and the power was gradually increased from 25 W to 75 W, during which the graphene covered MXene was exfoliated (see supplemental video). Then the system was shut down and the exfoliated samples were collected. The obtained samples were denoted as MXene@rGO.

Supplementary video related to this article can be found at https://doi.org/10.1016/j.ensm.2019.04.029.

2.5. Fabrication of all-solid-state flexible supercapacitors

Carbon cloth (MPL, Fuel Cell Earth Inc.) served as the current collector was cut into 2 × 1 (length × width) cm^2 pieces and cleaned with ethanol, acetone, and distilled water in turn followed by drying in an oven at 60 °C. The cleaned carbon cloth was then treated by oxygen plasma for 90 s under 75 W at a pressure of 2 Torr to improve the hydrophilicity. The electrode materials made of MXene@rGO, acetylene black and PVDF with a mass ratio of 8:1:1 was mixed in N-Methyl-2-pyrrolidone solvent (NMP, Fisher Scientific Inc.) under stirring for 12 h to obtain a homogeneous mixture, which was then transferred into an airbrush container (G222, Master Airbrush) with a 0.3 mm nozzle. The carbon cloth pieces were placed in parallel with a cover that left an open area of 1 × 1 (length × width) cm^2 for casting the electrode materials. Then, the electrode materials were sprayed by the airbrush, driven by a pressure of 60 psi, onto the exposed surface of the carbon cloth for 5 times with ~10 s pause between each round. The distance between the carbon cloth and nozzle was ~8 cm. The prepared electrodes were subsequently dried in an oven at 60 °C for 12 h. PVA-H_2SO_4 served as the electrolyte, which was prepared by 1) adding 2 g polyvinyl alcohol (PVA, Fisher Scientific Inc.) to 20 ml DI water and heating to 100 °C until the PVA fully dissolved to form a clear solution; 2) lowering the temperature to 85 °C and then dropwise adding 2 g H_2SO_4 under stirring for 2 h. The prepared gel electrolyte was dropped on top of the electrode materials to fully cover the electrode surfaces. Then, the electrodes were put into a fume hood for 12 h to allow the electrolyte to cure into semisolid. The electrodes were paired face to face and pressed together. The edges were sealed with silicon glue and the exposed carbon cloth was used for convenient connection in the electrochemical measurements. Devices using only the carbon cloth were also fabricated in the same procedures.

2.6. Physical characterization

The crystal structure of the samples was characterized by X-ray diffraction (XRD) (Rigaku Smartlab, Rigaku Americas, Inc. USA). The morphologies and structures were examined by transmission electron
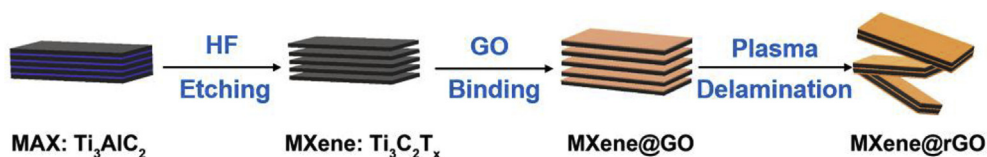
Fig. 1. Schematic illustration of MXene@rGO synthesis with structures evolution.
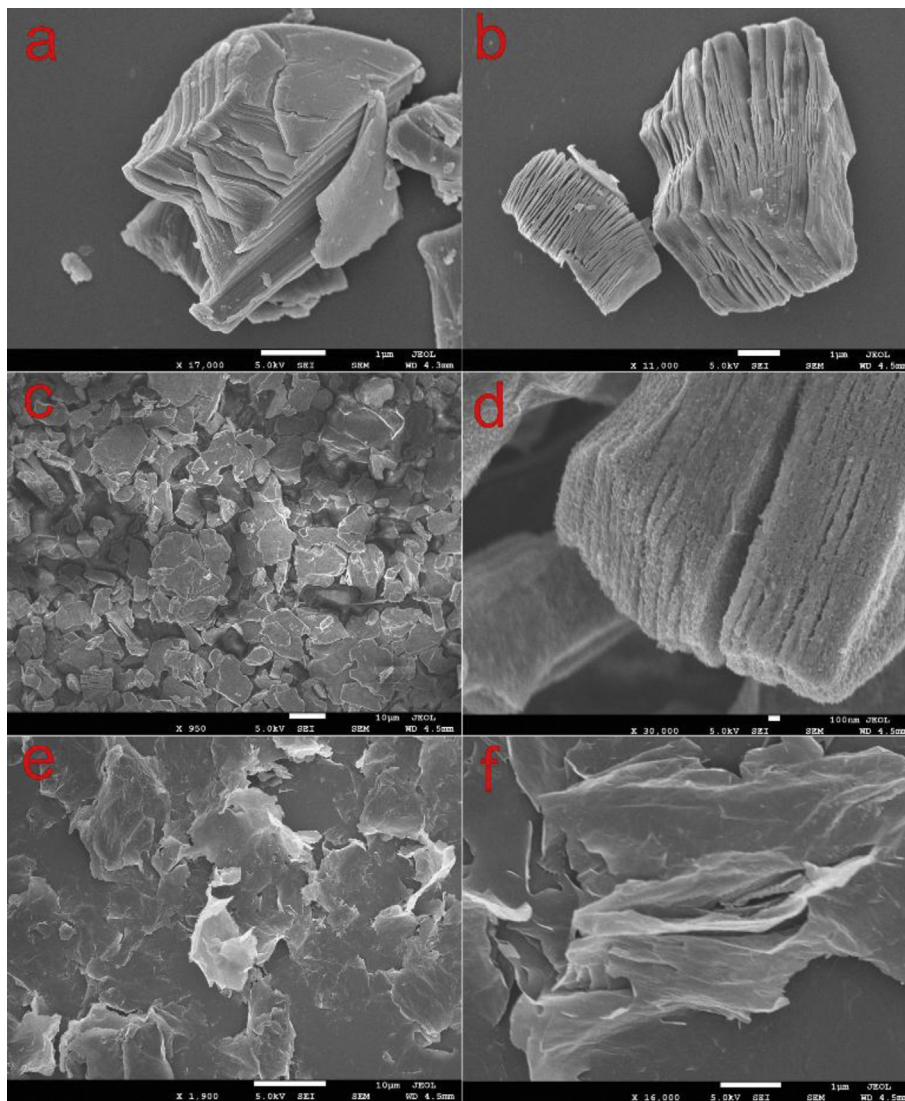

Fig. 2. SEM images of MAX (a), MXene (b), MXene@GO (c,d), and MXene@rGO (e,f).

microscopy (TEM) (JEM-2200FS, JEOL, Japan) at an acceleration voltage of 200 kV and a field emission scanning electron microscope (SEM) (JSM-7500F, JEOL, Japan) equipped with energy dispersive spectrum (EDS). X-ray photoelectron spectroscopy (XPS) was performed on an SSX-100 system (Surface Science Laboratories, Inc.) equipped with a mono-chromated Al K_α X-ray source.

2.7. Electrochemical characterization

All the electrochemical measurements, including cyclic voltammetry (CV) and electrochemical impedance spectroscopy (EIS), were conducted by a potentiostat (PGSTAT128N, Metrohm). The charge/discharge stability was measured by a battery charge/discharge system (BTS series, NEWARE, China).

3. Results and discussion

Fig. 1 schematically illustrates the fabrication of the MXene@rGO composite through CH_4 plasma treatment. MAX phase Ti_3AlC_2 is selected as the raw material. The subsequent HF etching creates layered $Ti_3C_2T_x$. After binding with GO colloid, freestanding paper-like sheets can be obtained from tiled MXene@GO gel upon natural drying (see Fig. S1a). The MXene@GO flakes are then exfoliated into fluffy MXene@rGO powders (see Fig. S1b) using CH_4 plasmas. The exfoliation process is swift and takes only a few seconds once the plasma excitation power reaches a threshold point, which is visible in the recorded video (see supplementary video).

The evolution of the microstructures from MAX through MXene to MXene@rGO was first evaluated using SEM. Typical dense layered chunk
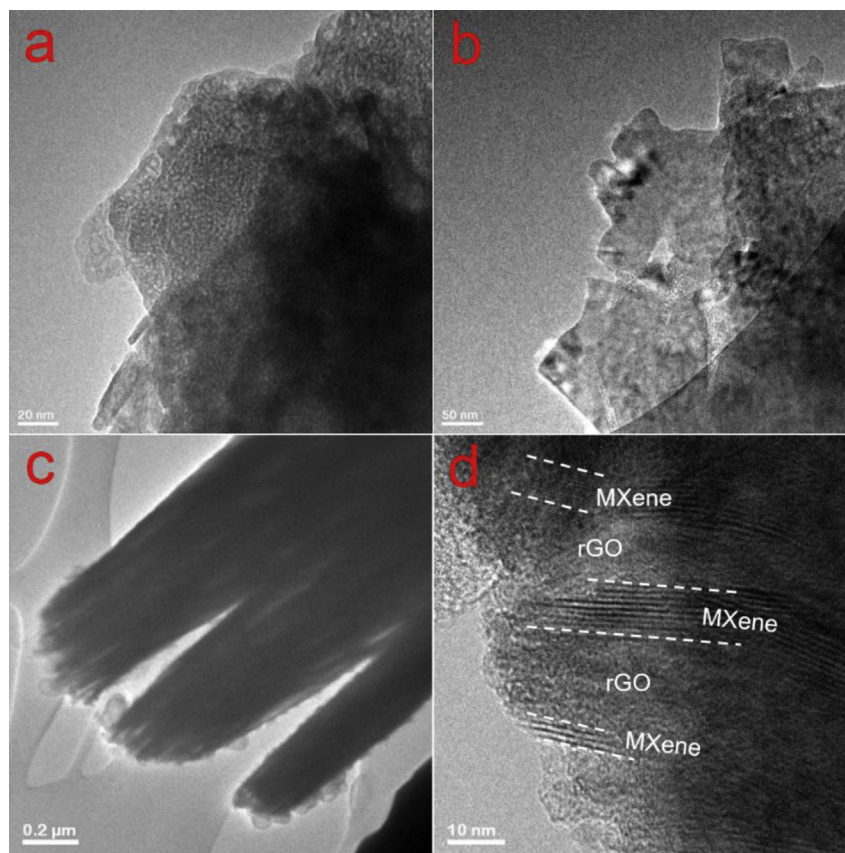
Fig. 3. TEM images of MAX (a), MXene (b) and MXene@rGO (c, d).

morphology of MAX was obtained as illustrated in Fig. 2a. EDS element mapping revealed uniform distribution of Ti, Al, and C (Fig. S2). After HF etching, layered structures with distinct spacing were observed (Fig. 2b) and the morphology was significantly different from that of MAX due to the removal of Al. Element mapping by EDS further indicated the removal of Al as well as the presence of F and O, which originated from the surface termination with F, O and OH groups (Fig. S3). Note that the signals of Si and Pt in EDS came from the Si substrate and the sputtered Pt, respectively. The above changes suggested the multilayer MXene was successfully prepared. After GO binding, the MXene@GO flakes distributed with random orientations (Fig. 2c). Besides, the layered structures of GO and MXene were observed in the cross-section images of MXene@GO flake (Fig. S4). Under high magnifications, the GO covered MXene could be observed (Fig. 2d), where a rough surface together with mostly closed spacing for MXene@GO could be observed. Meanwhile, it was noticed

that C signals were much stronger between MXene pieces in the element mapping (Fig. S5), which further indicated the binding function of GO. After the plasma exfoliation, the previous chunks of multilayered MXene became MXene@rGO in powders of thin pieces (Fig. 2e and f). In element mapping (Figs. S6a–e), C was observed over the resulting sample surfaces, which supported the expected wrapping effect. In EDS analysis (Fig. S6f), Ti, C, F, and O were detected in MXene@rGO, but the oxygen was believed to arise from the functional groups of MXene since GO had been reduced during plasma exfoliation according to our previous studies [37,38]. As proven previously, oxygen gas was formed during a plasma exfoliation of GO. The same principle applied to MXene@GO. Here, GO not only acted as a binder and expanding agent, but also led to the formation of graphene wrapped MXene. The plasma exfoliation was much more efficient than the other reported methods. As the GO was simultaneously reduced into graphene, the resulting materials can be directly
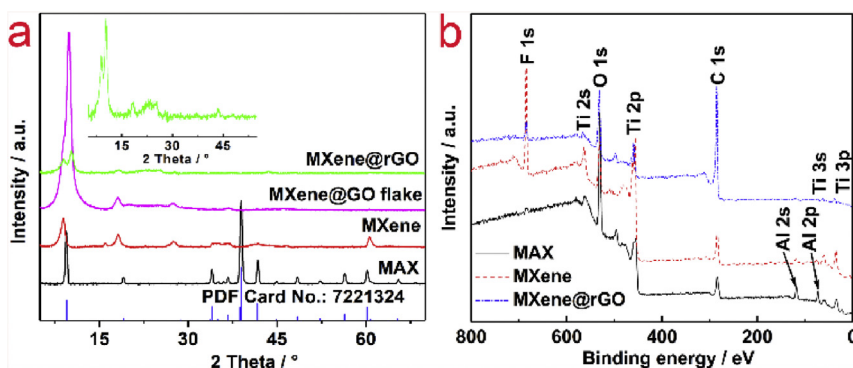

Fig. 4. XRD patterns (a) of MAX, MXene, MXene@GO and MXene@rGO; Inset is the individual XRD patterns of MXene@rGO; XPS survey (b) of MAX, MXene and MXene@rGO.
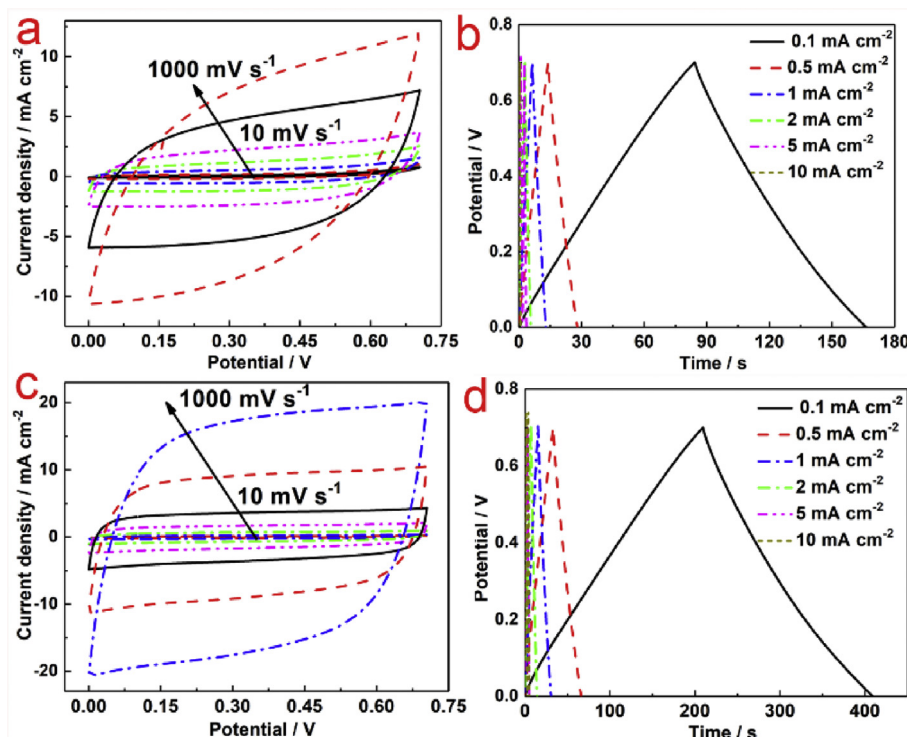
Fig. 5. CV and galvanostatic charge/discharge curves of MXene (a, b) and MXene@rGO (c, d).

used for making electrodes without any further processing.

To further characterize the microstructures of the samples, high-resolution TEM was performed. As shown in Fig. 3a, the MAX phase exhibited dense and thick morphologies with blurry edges. HF etching created thin layers at edges (Fig. 3b). After introducing GO and exfoliating with CH_4 plasmas, a hierarchical structure with graphene layer covering on dense MXene skeleton are clearly observed (Fig. 3c and d). To distinct from each other, it is noted that the interplanar spacing is about 13 Å, which is expected for MXene and is significantly different from that of graphene (3.45 Å). This result was in agreement with the SEM observations and further proved the graphene wrapped MXene structures. Based on the microstructure analysis, a distinct 2D layered structure was created and was expected to greatly facilitate the transport of the electrolyte ions to the MXene@rGO surfaces and promote the capacitance performance.

The evolution of the crystal structures of the samples was investigated using XRD. As shown in Fig. 4a, the diffraction patterns of MAX perfectly matched the indexed standard diffraction pattern (PDF card NO. 7551324). After HF etching, the typical peaks (002) and (004) located at 9.4° and 18.9° for pristine MAX shifted downward to 8.8° and 18.1°, respectively, and became broader with lower intensity. These changes indicated an increased c-lattice parameter in the MXene samples. In addition, the peaks located at 33.7°, 34.0°, 35.0°, 36.7°, 38.4°, 38.9°, 41.6°, 44.7°, 48.2°, 52.0° and 56.1°, which corresponded to (100), (101), (102), (103), (008), (104), (105), (106), (107), (108) and (109) planes of MAX, either vanished or became broader peaks, suggesting the successful removal of Al after HF etching. These results indicated that MXene was successfully prepared with increased spacing in between the layers, which were in agreement with the electron microscopy analysis. A prominent peak located at 10° with a shoulder at ~8.8° could be observed in the diffraction pattern of the MXene@GO flakes, which was attributed to (001) planes of GO and (002) crystal planes of MXene. Additionally, the other typical peaks of MXene remained after adding GO, indicating the skeleton of MXene was preserved and bonded with GO. After CH_4 plasma treatment, a broad peak located at 24° corresponding to the (002) crystal plane of rGO emerged (see inset) in the

MXene@rGO diffraction pattern. This demonstrated the decreased d-spacing due to the absence of oxygen in the graphene interlayers and the evolution from GO to rGO [40]. Overall, the structural evolution observed by XRD was consistent with the results of SEM and TEM, indicating the successful preparation of MXene, MXene@GO, and MXene@rGO.

XPS analysis was performed to understand the chemical valence of the elements in the materials. Ti, Al, and C were detected in the XPS survey spectrum of MAX (Fig. 4b), but the Al signal disappeared and O and F emerged in the spectra of MXene and MXene@rGO. These results further manifested the successful removal of Al from MAX and the formation of functional groups after HF etching. The Ti 2p high-resolution spectrum of MAX (Fig. S7a) revealed six peaks located at ~454.06, 454.67, 455.72, 458.40, 460.19 and 464.12 eV, corresponding to the bonding status of Ti—Al, Ti—C, Ti(II) oxide, Ti—O, Ti(II) and Ti—O, respectively [41–45]. On the other hand, the Ti 2p spectrum of MXene (Fig. S7b) could be deconstructed into four sets of doublets ($2p_{3/2}$ and $2p_{1/2}$) at 454.6/460.3, 456.4/461.5, 457.0/462.4 and 458.8/464.4 eV, which were assigned to Ti—C, Ti (II), Ti (III) and Ti (IV), respectively [30, 41,44,45]. After CH_4 plasma exfoliation, there were three doublets of Ti $2p_{3/2}$ and $2p_{1/2}$, which can be assigned to Ti—C, Ti (II), and Ti—O bonds, respectively [46,47]. Overall, the evolution of the chemical bonding from MAX to MXene@rGO revealed compositions and structures of the materials.

All-solid-state flexible supercapacitors with PVA-H_2SO_4 electrolyte were fabricated to evaluate the electrochemical performance of MXene@rGO in energy storage. The electrochemical characteristics of the assembled devices were evaluated by CV, EIS, and charge/discharge in a two-electrode configuration. The CV measurements were conducted at different scanning rates ranging from 10 to 1000 mV s^{-1} for the MXene and the MXene@rGO electrodes, respectively. Both materials showed regular CV curves (Fig. 5a and c), implying good electrical-double-layer-capacitance behavior and electrochemical reversibility. The MXene@rGO electrodes exhibited much better capacitance performance than the MXene electrodes as evidenced by 1) ideal rectangular CV curves even at a high scanning rate up to 1,000 mV s^{-1} in comparison with the
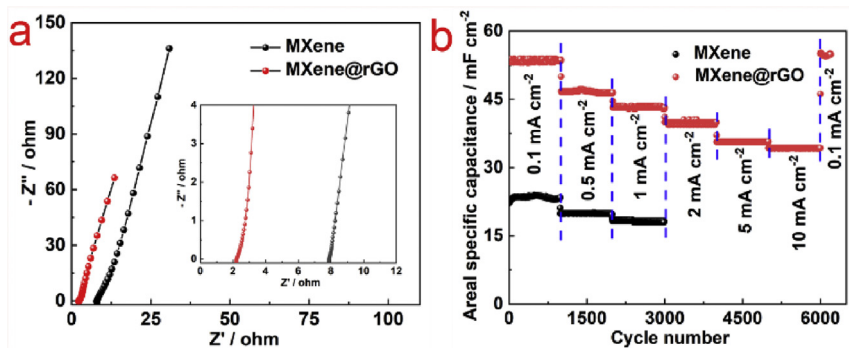
Fig. 6. Nyquist plots (a) and charge/discharge cycles (b) of MXene and MXene@rGO (e,f).

distorted curves of the MXene, and 2) much higher current density at different scanning rates. Galvanostatic charge/discharge measurements were also performed to further evaluate the capacitance performance. As shown in Fig. 5b and d, symmetric triangle curves during charge/discharge at different current densities were observed for both the electrodes, indicating the formation of an electrochemical double layer and fast intercalation/de-intercalation of ions between MXene@rGO nanosheets. CV test was also conducted for devices made of symmetric carbon cloth alone to exclude the capacitance contributed from the substrate (Fig. S8a); the current density was nearly negligible as compared to that of MXene and MXene@rGO electrodes. The specific capacitances of the devices were determined from constant current charge/discharge curves using the following equation [48]:

$$C_A = \frac{2I \times \Delta t}{\Delta V \times S}$$

where C_A (F cm^{-2}) is the areal specific capacitance, I (A) is the constant discharge current, Δt (s) is the discharge time, ΔV (V) is the potential window, and S (cm^2) is the area of the electrodes. At different charge/discharge currents ranging from 0.1 to 10 mA cm^{-2}, the areal specific

capacitance was 54, 47, 43, 40, 36, and 35 mF cm^{-2}, respectively, for MXene@rGO, which preserves ~65% of the capacitance even at a high current density of 10 mA cm^{-2}. The specific areal capacitance of MXene@rGO was considerably higher than that of MXene, being 24, 20 and 18 mF cm^{-2} at current densities of 0.1, 0.5 and 1 mA cm^{-2}, respectively. Meanwhile, the specific areal capacitance of bare carbon cloth was 2.9 mF cm^{-2} at current densities of 0.5 mA cm^{-2}, which was far smaller than that of MXene and MXene@rGO at the same condition, indicating again that the contribution from the substrate was negligible (Fig. S8b).

The Nyquist plots for the MXene and the MXene@rGO electrodes were also evaluated (Fig. 6a). The electrochemical impedance spectra (*EIS*) conducted in a frequency range of 10 mHz–100 kHz consisted of two regions with an *x*-intercept, a semicircle, and a spike at a high and low frequency, respectively. The *x*-intercept and an inconspicuous deformed semicircle at the high frequency region could be assigned to bulk electrolyte resistance (R_s, 8.0 and 2.2 Ω for MXene and MXene@rGO, respectively) and charge-transfer resistance (R_{ct}, 0.1 Ω for MXene and 98.2 Ω MXene@rGO), while the slope of the straight line at the low-frequency region, also called *Warburg* line, was attributed to *Warburg* resistance (Z_w), which represented the electrolyte diffusion to
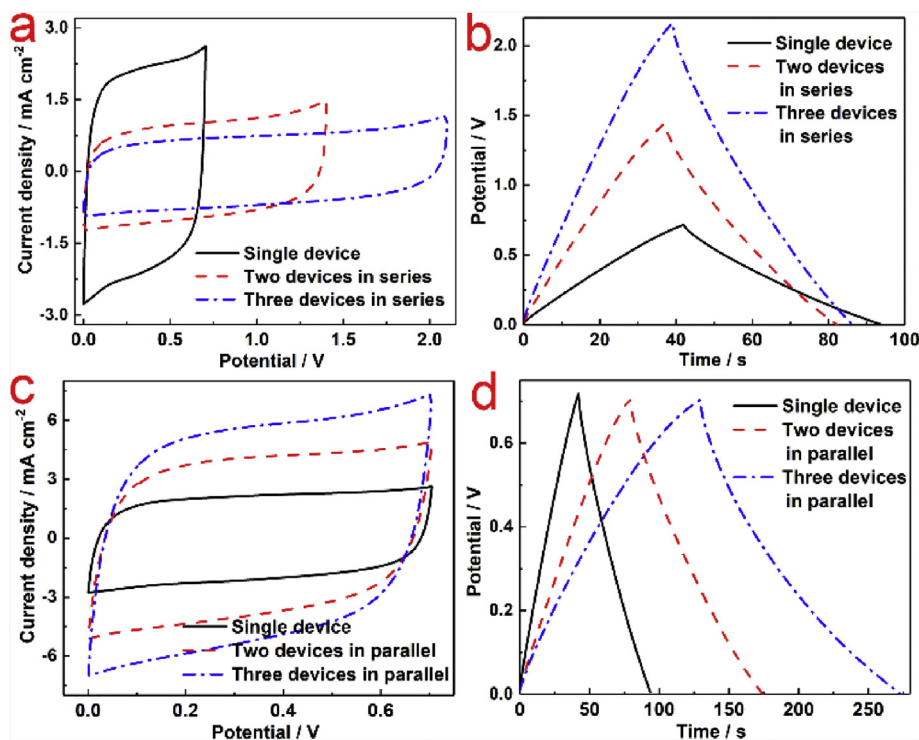

Fig. 7. CV (a, c) and galvanostatic charge/discharge curves (b, d) of one, two, and three devices in series and parallel, respectively.
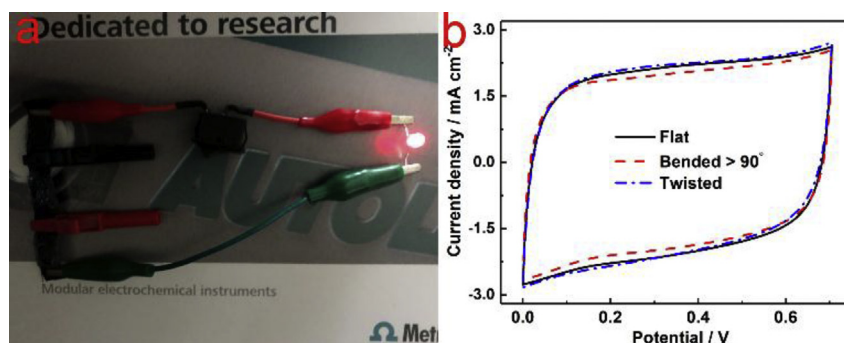
Fig. 8. Powered red LED by three devices connected in series (a) and CV curves of devices under different deformation and digital photography (b).

the electrode surface [49,50]. The simulated equivalent circuit is shown in Fig. S9, consisting of C_{dl} and C_f for double layer capacitance and faradaic capacitance, respectively, besides the elements described here-inbefore [49–51]. It was noted that the MXene@rGO electrode showed a much smaller resistance (13.6 Ω) than that of MXene (35.8 Ω), which was attributed to the rGO wrapped on MXene because rGO was known as an excellent electrode material with superior conductivity.

The stability of the supercapacitors fabricated with MXene and MXene@rGO electrodes was evaluated by life cycle measurements at different current densities. As presented in Fig. 6b, both MXene and MXene@rGO electrodes showed almost 100% retention in each individual 1000 cycles. However, MXene@rGO exhibited much larger capacitance at all current densities than that of MXene. MXene@rGO still possessed the same capacitance performance of the first 1000 cycles at the same current density after a total of 6000 cycles.

For practical applications in energy storage, two and three of the fabricated all-solid-state flexible supercapacitors using the MXene@rGO electrodes were connected in series and parallel, respectively. As shown in Fig. 7a, almost ideal rectangular shape CV curves (scanning rate: $100\,mV\,s^{-1}$) and symmetric triangle charge/discharge curves (current density: $0.5\,mA\,cm^{-2}$) with extended voltage window up to 2.1 V were obtained for the serial devices. On the other hand, the devices connected in parallel provided about 3 times higher current density with regular rectangular CV curves and symmetric triangular charge/discharge curves.

A real application of the fabricated devices is illustrated in Fig. 8a, where a simple circuit was built with an LED load. The LED was lit up for over 5 min after the supercapacitors were charged for <10 s, showing promising potential to meet the need for fast charging of electronic devices. The mechanical flexibility of the fabricated devices was evaluated under manual deformations. Except a little drop in the current density (Fig. 8b), no distortion in the CV curves was observed when the device was bent or twisted over 90°. These results indicated the potential mechanical flexibility and stable electrochemical performance of the fabricated devices.

4. Conclusion

Graphene wrapped MXene 2D materials, denoted as MXene@rGO, are successfully prepared *via* facile plasma exfoliation and used in all-solid-state flexible supercapacitors. GO can be incorporated into MXene as a binder and expansion agent to form MXene@GO composite. CH_4 plasma exfoliation of MXene@GO creates graphene wrapped MXene that leads to excellent capacitance performance of supercapacitors. In comparison with the MXene electrodes, the graphene wrapped MXene leads to much higher specific areal capacitance of $54\,mF\,cm^{-2}$ at $0.2\,A\,cm^{-2}$, lower resistance of 13.6 Ω, and excellent capacitance retention of ~100% in every 1000 individual cycles. In addition to the superior mechanical flexibility, the MXene@rGO based all-solid-state supercapacitors can be connected in series and parallel to power electronic devices.

Appendix A. Supplementary data

Supplementary data to this article can be found online at https://doi.org/10.1016/j.ensm.2019.04.029.

References

[1] Y.S. Rim, S.H. Bae, H. Chen, N. De Marco, Y. Yang, Adv. Mater. 28 (2016) 4415–4440.
[2] G. Nyström, A. Marais, E. Karabulut, L. Wågberg, Y. Cui, M.M. Hamedi, Nat. Commun. 6 (2015) 7259.
[3] X. Peng, L. Peng, C. Wu, Y. Xie, Chem. Soc. Rev. 43 (2014) 3303–3323.
[4] X. Lu, M. Yu, G. Wang, Y. Tong, Y. Li, Energy Environ. Sci. 7 (2014) 2160–2181.
[5] Z. Peng, J. Lin, R. Ye, E.L. Samuel, J.M. Tour, ACS Appl. Mater. Interfaces 7 (2015) 3414–3419.
[6] Y. Rangom, X. Tang, L.F. Nazar, ACS Nano 9 (2015) 7248–7255.
[7] B. Li, F. Dai, Q. Xiao, L. Yang, J. Shen, C. Zhang, M. Cai, Energy Environ. Sci. 9 (2016) 102–106.
[8] M. Rose, Y. Korenblit, E. Kockrick, L. Borchardt, M. Oschatz, S. Kaskel, G. Yushin, Small 7 (2011) 1108–1117.
[9] D. Choi, G.E. Blomgren, P.N. Kumta, Adv. Mater. 18 (2006) 1178–1182.
[10] S. Chen, J. Zhu, X. Wu, Q. Han, X. Wang, ACS Nano 4 (2010) 2822–2830.
[11] C.-C. Hu, K.-H. Chang, M.-C. Lin, Y.-T. Wu, Nano Lett. 6 (2006) 2690–2695.
[12] V. Ganesh, S. Pitchumani, V. Lakshminarayanan, J. Power Sources 158 (2006) 1523–1532.
[13] J.J. Yoo, K. Balakrishnan, J. Huang, V. Meunier, B.G. Sumpter, A. Srivastava, M. Conway, A.L. Mohana Reddy, J. Yu, R. Vajtai, Nano Lett. 11 (2011) 1423–1427.
[14] M. Oschatz, S. Boukhalfa, W. Nickel, J.P. Hofmann, C. Fischer, G. Yushin, S. Kaskel, Carbon 113 (2017) 283–291.
[15] P.J. Hanumantha, M.K. Datta, K. Kadakia, C. Okoli, P. Patel, P.N. Kumta, Electrochim. Acta 207 (2016) 37–47.
[16] P. Xu, B. Wei, Z. Cao, J. Zheng, K. Gong, F. Li, J. Yu, Q. Li, W. Lu, J.-H. Byun, ACS Nano 9 (2015) 6088–6096.
[17] S. Mohajernia, S. Hejazi, A. Mazare, N.T. Nguyen, I. Hwang, S. Kment, G. Zoppellaro, O. Tomanec, R. Zboril, P. Schmuki, Mater. Today Energy 6 (2017) 46–52.
[18] M. Naguib, M. Kurtoglu, V. Presser, J. Lu, J. Niu, M. Heon, L. Hultman, Y. Gogotsi, M.W. Barsoum, Adv. Mater. 23 (2011) 4248–4253.
[19] M. Naguib, O. Mashtalir, J. Carle, V. Presser, J. Lu, L. Hultman, Y. Gogotsi, M.W. Barsoum, ACS Nano 6 (2012) 1322–1331.
[20] S. Kajiyama, L. Szabova, H. Iinuma, A. Sugahara, K. Gotoh, K. Sodeyama, Y. Tateyama, M. Okubo, A. Yamada, Adv. Energy Mater. 7 (2017) 1601873.
[21] B. Anasori, M.R. Lukatskaya, Y. Gogotsi, Nat. Rev. Mater. 2 (2017) 16098.
[22] X. Liang, A. Garsuch, L.F. Nazar, Angew. Chem. 127 (2015) 3979–3983.
[23] C.J. Zhang, V. Nicolosi, Energy Storage Mater. 16 (2018) 102–125.
[24] N.K. Chaudhari, H. Jin, B. Kim, D. San Baek, S.H. Joo, K. Lee, J. Mater. Chem. A 5 (2017) 24564–24579.
[25] J. Yan, C.E. Ren, K. Maleski, C.B. Hatter, B. Anasori, P. Urbankowski, A. Sarycheva, Y. Gogotsi, Adv. Funct. Mater. 27 (2017) 1701264.
[26] S. Lai, J. Jeon, S.K. Jang, J. Xu, Y.J. Choi, J.-H. Park, E. Hwang, S. Lee, Nanoscale 7 (2015) 19390–19396.
[27] J. Xu, J. Shim, J.H. Park, S. Lee, Adv. Funct. Mater. 26 (2016) 5328–5334.
[28] T. Hu, M. Hu, Z. Li, H. Zhang, C. Zhang, J. Wang, X. Wang, Phys. Chem. Chem. Phys. 18 (2016) 20256–20260.

[29] X. Xie, M.-Q. Zhao, B. Anasori, K. Maleski, C.E. Ren, J. Li, B.W. Byles, E. Pomerantseva, G. Wang, Y. Gogotsi, Nano Energy 26 (2016) 513–523.

[30] O. Mashtalir, M. Naguib, V.N. Mochalin, Y. Dall'Agnese, M. Heon, M.W. Barsoum, Y. Gogotsi, Nat. Commun. 4 (2013) 1716.

[31] O. Mashtalir, M.R. Lukatskaya, M.Q. Zhao, M.W. Barsoum, Y. Gogotsi, Adv. Mater. 27 (2015) 3501–3506.

[32] M. Naguib, R.R. Unocic, B.L. Armstrong, J. Nanda, Dalton Trans. 44 (2015) 9353–9358.

[33] M. Boota, B. Anasori, C. Voigt, M.Q. Zhao, M.W. Barsoum, Y. Gogotsi, Adv. Mater. 28 (2016) 1517–1522.

[34] Y. Tian, C. Yang, W. Que, X. Liu, X. Yin, L.B. Kong, J. Power Sources 359 (2017) 332–339.

[35] K. Wang, M. Xu, M. Shrestha, Z. Gu, Q.H. Fan, Mater. Today Energy 4 (2017) 7–13.

[36] M.Q. Zhao, C.E. Ren, Z. Ling, M.R. Lukatskaya, C. Zhang, K.L. Van Aken, M.W. Barsoum, Y. Gogotsi, Adv. Mater. 27 (2015) 339–345.

[37] K. Wang, M. Xu, Y. Gu, Z. Gu, J. Liu, Q.H. Fan, Nano Energy 31 (2017) 486–494.

[38] K. Wang, B. Zheng, M. Shrestha, T. Schuelke, Q.-H. Fan, Energy Storage Mater. 14 (2018) 230–237.

[39] W.S. Hummers Jr., R.E. Offeman, J. Am. Chem. Soc. 80 (1958), 1339-1339.

[40] M. Fu, Q. Jiao, Y. Zhao, J. Mater. Chem. A 1 (2013) 5577–5586.

[41] B. Dai, B. Zhao, X. Xie, T. Su, B. Fan, R. Zhang, R. Yang, J. Mater. Chem. C 6 (2018) 5690–5697.

[42] S. Myhra, J. Crossley, M. Barsoum, J. Phys. Chem. Solids 62 (2001) 811–817.

[43] O. Wilhelmsson, J.-P. Palmquist, E. Lewin, J. Emmerlich, P. Eklund, P.Å. Persson, H. Högberg, S. Li, R. Ahuja, O. Eriksson, J. Cryst. Growth 291 (2006) 290–300.

[44] M.C. Biesinger, L.W. Lau, A.R. Gerson, R.S.C. Smart, Appl. Surf. Sci. 257 (2010) 887–898.

[45] D. Mencer Jr., T. Hess, T. Mebrahtu, D. Cocke, D. Naugle, J. Vac. Sci. Technol. A 9 (1991) 1610–1615.

[46] M. Ghidiu, J. Halim, S. Kota, D. Bish, Y. Gogotsi, M.W. Barsoum, Chem. Mater. 28 (2016) 3507–3514.

[47] R.B. Rakhi, B. Ahmed, M.N. Hedhili, D.H. Anjum, H.N. Alshareef, Chem. Mater. 27 (2015) 5314–5323.

[48] Y. Yang, Q. Huang, L. Niu, D. Wang, C. Yan, Y. She, Z. Zheng, Adv. Mater. 29 (2017) 1606679.

[49] Y. Mun, C. Jo, T. Hyeon, J. Lee, K.-S. Ha, K.-W. Jun, S.-H. Lee, S.-W. Hong, H.I. Lee, S. Yoon, Carbon 64 (2013) 391–402.

[50] S. Hu, S. Zhang, N. Pan, Y.-L. Hsieh, J. Power Sources 270 (2014) 106–112.

[51] Z. Fan, J. Yan, T. Wei, L. Zhi, G. Ning, T. Li, F. Wei, Adv. Funct. Mater. 21 (2011) 2366–2375.